Influence of Mn doping on structural, optical, and magnetic properties of BiFeO$_3$ films fabricated by the sol-gel method

Mariyemu Wushuer, Fuerkaiti Xiaerding[*]**, Mamatrishat Mamat**[*]**, Ma Xu, Abuduwaili Mijiti, Litipu Aihaiti**

School of Physics and Technology, Xinjiang University, Urumqi, Xinjiang 830046 China

[*]Corresponding authors, e-mail: 3549598778@qq.com (F. Xiaerding), mmtrxt@xju.edu.cn (M. Mamat)

ABSTRACT: The present study synthesized BiFe$_{1-x}$Mn$_x$O$_3$ ($x = 0.00$, 0.03, 0.05 and 0.07) films by the sol-gel method. Rhombohedral lattice structure and phase transition are confirmed by X-ray diffraction and Raman spectroscopy. Scanning electron microscopy and atomic force microscopy images showed that with the increase of Mn content, the grain size and average roughness of the film first decreased and then increased. The saturated magnetization of the BiFe$_{1-x}$Mn$_x$O$_3$ ($x = 0.03$, 0.05 and 0.07) films was significantly enhanced compared with the BiFeO$_3$ film, thus indicating its potential applicability for information storage. Meanwhile, the Mn-doped films exhibited a reduced optical band gap. The results verify the applicability of the presented method in improving the performance of high-efficient photocatalysis.

KEYWORDS: sol-gel method, magnetic properties, optical properties, Mn doping, BiFeO$_3$ films

INTRODUCTION

Multiferroics are multifunctional materials that simultaneously possess two or more ferroic orders such as ferroelectric and ferromagnetic [1]. With the continuous development of science and technology, multiferroic materials have been widely used in electronic devices and in various smart devices such as spintronics, magnetoelectric memory and piezotronics [2]. Room-temperature multiferroic Bismuth Ferrite BiFeO$_3$ (BFO) is a rhombohedral distorted ferroelectric perovskite with space group R3c below the Curie temperature (T$_C$ ≈ 1100 K) and shows antiferromagnetic behavior below the Néel temperature (T$_N$ ≈ 643 K) [3]. However, the special magnetic cycloidal spiral arrangement for Fe^{3+}, which has a long cycle length of 60–64 nm [4] and results in nearly zero macroscopic magnetization [5, 6], generated the performance of bulk BFO for the technological applications is not satisfied for magnetic requirements. Moreover, in recent years, researchers have found that BFO not only has a small optical band gap (2.2–2.9 eV) but also possesses favorable nonlinear optical properties, thus widening the application of BFO [7]. Therefore, further examination of the optical, magnetic and structural properties of BFO films to improve its performance is worthwhile [8].

Various methods have been used for the preparation of BFO films, including of magnetron sputtering [9], hydrothermal method [10] and sol-gel method [11]. However, the sol-gel method is one of the simpler methods used in the preparation of thin films due to its straightforward composition control, large area coatings and inexpensive equipment costs. The preparation of BFO films with the sol-gel method focuses on properties improvement via rare-earth and transition metals substitution at the A- and B-sites, respectively [12, 13]. Doping of various Lanthanide ions (Gd^{3+}) [14], Sm^{3+} [3] and Nd^{3+} [15] at the Bi^{3+} site of BFO has been reported to improve the magnetic and ferroelectric properties via suppression of the spiral spin structure and reduction of oxygen vacancies. Meanwhile, B-site ordering of the transition-metal ions has exhibited the ability to generate ferromagnetic or ferrimagnetic BFO materials. Similarly, doping of the transition metal ions Zn^{2+} [16], Mn^{2+} [8], Ni^{2+} [5] and Mg^{2+} [17] at the Fe^{3+} site of BFO has also enhanced its magnetic and ferroelectric properties [18]. The replacement of ions at the A site at different ionic radii can readjust the structure to reduce the leakage current, as well as increase polarization [19]. Furthermore, substitution at the A site can increase the magnetism by releasing suppressed spiral spin

modulation of the G-type antiferromagnetism [20]. Although, intensive research works have reported the ferro-electric and magnetic properties of BFO films by adjusting the Mn doping concentration, the optical properties and surface roughness morphologies require further investigation. The present work first grew $BiFe_{1-x}Mn_xO_3$ ($x = 0.00, 0.03, 0.05$ and 0.07) films on SiO_2/Si substrates by the sol-gel method. Then, structures, surface morphologies, and optical and magnetic properties of the samples were investigated. In particular, the optical properties of the BFMO films were studied based on their absorption spectra.

MATERIALS AND METHODS

Pure BFO and transition metal Mn-doped BFO films were prepared by the sol-gel method. Bismuth (III) nitrate pentahydrate $[Bi(NO_3)_3 \cdot 5H_2O]$ (5% excess to compensate for the loss of Bi due to evaporation during the post-annealing process), Ferric (III) nitrate nonahydrate $[Fe(NO_3)_3 \cdot 9H_2O]$ and Manganese acetate $[C_4H_6MnO_4(Mn(CH_3COO)_2)]$ were used as the raw materials. Ethylene glycol methyl ether and glacial acetic acid were used as solvents. Twenty milliliters of a 0.325 mol/l solution of every doping amount were then prepared. Then, the solution was magnetically stirred for 3 h and kept at room temperature for 24 h. In this work, the SiO_2/Si substrate was sequentially cleaned with acetone, ethanol, and deionized water for 5 min. Furthermore, the precursor solution was spin-coated on the SiO_2/Si substrate at a spinning speed of 4000 rpm for 20 s. Subsequently, the spin-coated wet film was preheated on a hot plate at 200 °C for 5 min. The coating process was repeated 15 times. Finally, the obtained film was annealed in air at a temperature of 550 °C for 10 min.

The $BiFe_{1-x}Mn_xO_3$ (BFMO) film crystal structures and phase purity were identified by X-ray diffractometry (XRD, Bruker D2, D8 Advance, Germany) with CuKα rays at a wavelength of 1.5418 Å, and within an XRD profile range of 20°–60°. The surface morphologies of the BFMO films were characterized by scanning electron microscopy (SEM, SU8010, HITACHI, Japan) and atomic force microscopy (AFM, Dimension Icon, Germany), respectively. Raman spectra of samples were measured via Raman spectrometry (AES, iHR550, Horiba, France). The optical properties of the BFMO films were measured by UV-visible spectrophotometry (UV-vis, UV/vis Lambda 650, Perkin Elmer Company, Waltham, Massachusetts, USA). The magnetization of the samples were measured by vibrat-
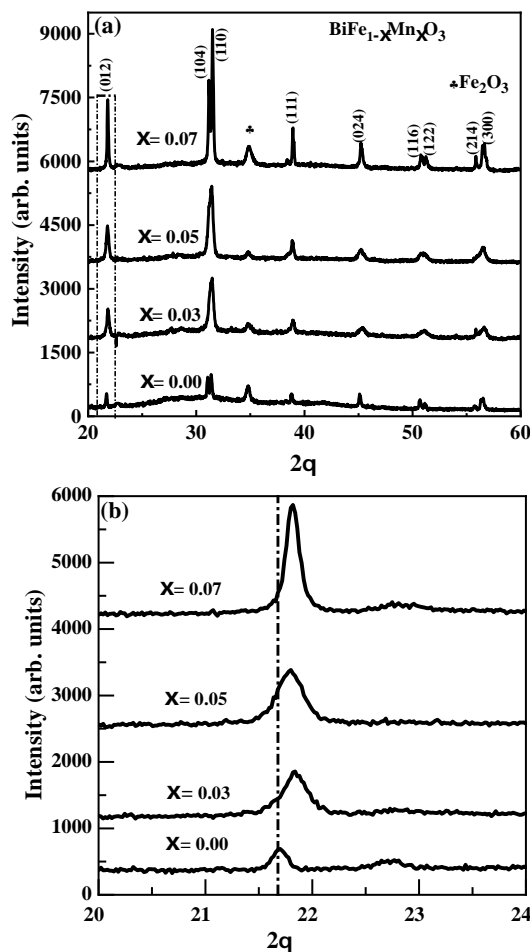

Fig. 1 (a) XRD spectra of $BiFe_{1-x}Mn_xO_3$ ($x = 0.00, 0.03, 0.05$ and 0.07) films. (b) The magnified XRD image of (101) peak for 2θ range of 20°–24°.

ing sample magnetometry (VSM, SQUID-MPMS-XL, American Quantum Design Company, USA).

RESULTS AND DISCUSSION

Fig. 1 shows the XRD spectra of the $BiFe_{1-x}Mn_xO_3$ ($x = 0.00, 0.03, 0.05$ and 0.07) films grown on the SiO_2/Si substrates. All of the peaks in the XRD spectra corresponded to a perovskite-type rhombohedral structure (PDF72-2321) that belonged to the R3c (160) space group. The XRD patterns confirm the presence of strong crystal plane in the (012), (104), (110), (111), (024), (116), (122), (214) and (300) directions, which fit into the main peaks of the $BiFe_{1-x}Mn_xO_3$ films. An increase in Mn doping increased the intensity of the diffraction peaks, indicating that Mn doping promoted crystallinity. For each sample, the average grain size was estimated
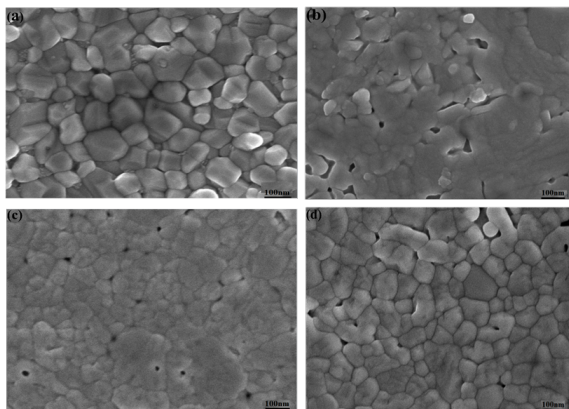
Fig. 2 SEM images of $BiFe_{1-x}Mn_xO_3$ films, where (a), (b), (c) and (d) are corresponding to $x = 0.00$, 0.03, 0.05 and 0.07, respectively.

using the Scherrer formula [21]. Doping contents of $x = 0.00$, 0.03 and 0.05 generated film grain sizes of 32.6 nm, 19.7 nm and 19.5 nm, respectively, indicating a contrasting trend between the grain size and doping content. A Mn doping amount of $x = 0.07$ exhibited an increase in the BFMO film grain size to 45 nm, suggesting that the grain size first decreased and then increased with the Mn doping amount, which agrees with a previous report [20]. According to Fig. 1(b), all of the peak positions of the BFMO films slightly shifted towards the right following an increase in the Mn concentration compared with BFO, which can be attributed to a small distortion in the crystal structure due to the smaller ionic radius of the Mn^{2+} ions (0.067 nm) partially substitute by the Fe^{3+} ions (0.087 nm). This result is in accordance with previous reports [22]. Moreover, the presence of impurity, such as Fe_2O_3, could be assigned to the high temperature that accelerated the volatilization of the Bi elements and reduced the content of Bi_2O_3, which resulted in an enriched Fe_2O_3 impurity phase [18].

Fig. 2 presents the surface morphologies of pure BFO and the BFMO films, which were measured by SEM. All of the samples exhibited good crystallinity. The average grain size of the samples first decreased and then increased with the increasing Mn content. Both the BFO and BFMO films ($x = 0.07$) exhibited well-crystallized microstructures and smooth surfaces. The BFMO films ($x = 0.03$ and 0.05) showed a gradually decreasing grain size and inhomogeneous surface micrographs. In this case, the crystal grains exhibited an irregular polyhedron. Additionally, more defects were formed at the grain
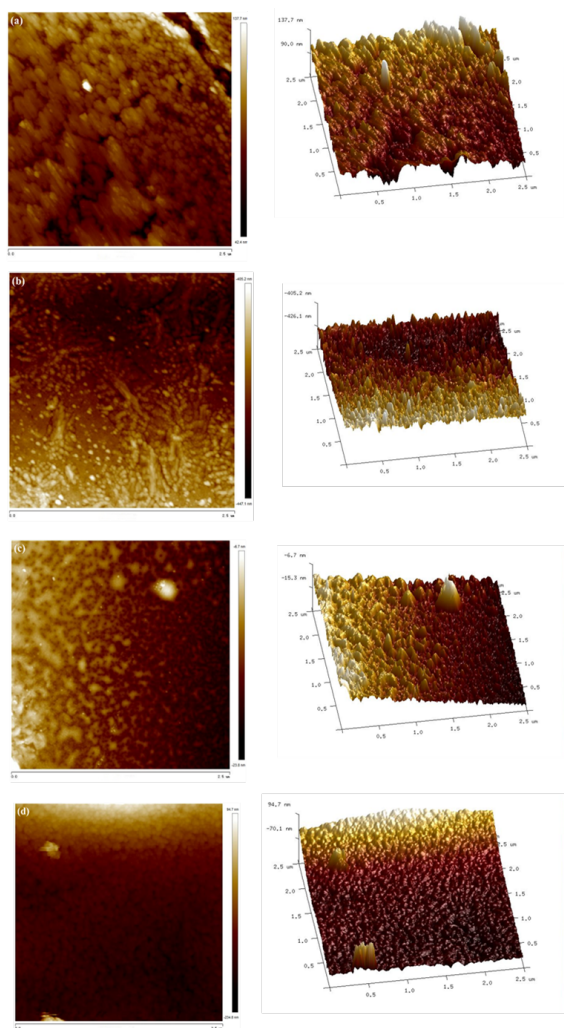

Fig. 3 The AFM images (2.5 μm × 2.5 μm) of $BiFe_{1-x}Mn_xO_3$ films, where (a), (b), (c) and (d) are corresponding to $x = 0.00$, 0.03, 0.05 and 0.07, respectively.

boundaries, resulting in a decrease in the grain size.

The surface topography and roughness of the BFMO films were characterized by AFM (Fig. 3). The average roughness (R_a) of the films was measured over an area of 2.5 μm × 2.5 μm, of which the BFMO films exhibited R_a values of 6.35 nm, 2.74 nm, 2.19 nm and 6.58 nm at Mn contents of $x = 0.0$, 0.03, 0.05 and 0.07, respectively. The R_a of the samples first decreased and then increased with the increasing Mn content. The AFM results indicated that Mn doping strongly affected the roughness of the BFMO films, which agrees well with the XRD spectra [23, 24].

Fig. 4(a) shows the Raman spectrum of pure BFO. Four A_1 modes at Raman shifts of 145, 180,
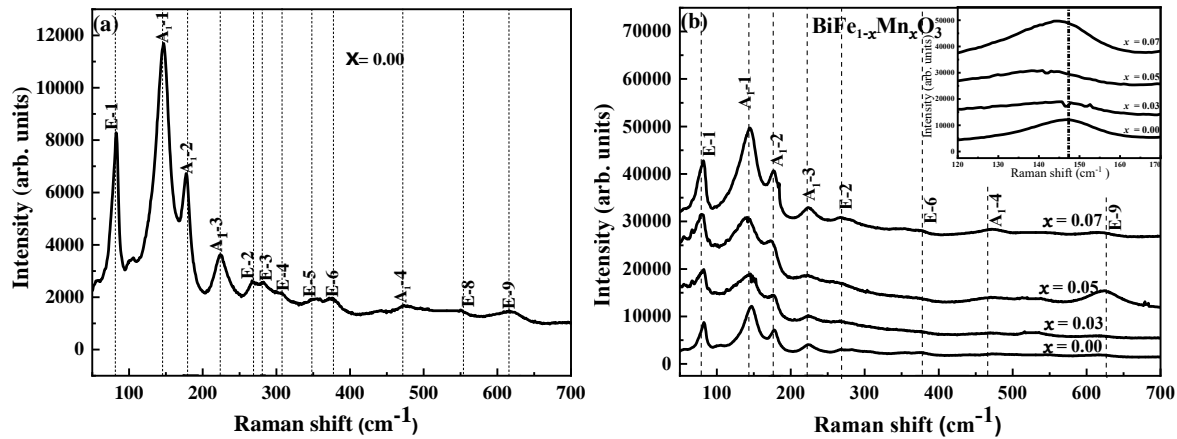
Fig. 4 Raman spectra of (a) pure $BiFO_3$ and (b) the Mn doped $BiFe_{1-x}Mn_xO_3$ ($x = 0.00$, 0.03, 0.05 and 0.07) films.

225 and 470 cm^{-1} and eight E-1 mode peaks at 82, 266, 285, 307, 354, 376, 549 and 619 cm^{-1} confirmed the structure of the BFO films [25]. However, only 12 active modes were observed, indicating the absence of one active mode (E-7). The absence of this particular Raman peak may be due to the higher local stress and the presence of point defects in the pure BFO sample [26]. However, the peak intensity increased and peaks slightly red shifted compared with pure BFO. The low-wave number Raman modes were governed by Bi−O vibration, and the high-wave number Raman modes were related to the Fe−O vibration [14, 25]. The intensity of A_1 mode increased with the Mn dopant, suggesting the chemical activity enhancement of the Bi−O isolation electron, which may be due to the local lattice distortion in the as-prepared samples [20]. In addition, certain Raman peaks exhibited changes in their relative widths, possibly due to the structure transition of the BFO lattice [22]. These results were also in accordance with the XRD results. Moreover, the insert in Fig. 4(b) presents the Raman peak of the [A_1-1] mode at 145 cm^{-1}, which was red-shifted with the increasing Mn substitution. This result can be attributed to the lower atomic weight of Mn (54.9 g/mol) compared with Fe (55.8 g/mol), since the frequency of the Raman modes was dependent on the force constant and ionic mass [27].

The magnetic hysteresis ($M − H$) loops of the BFMO films are shown in Fig. 5, which clearly indicate weak ferromagnetism for all of the films. A previous report correlated the weak ferromagnetism in BFO with the rhombohedral distorted perovskite structure (space group R3c), in which both ferroelectric atomic displacements and weak ferromagnetism were allowed [28]. The inset shows the
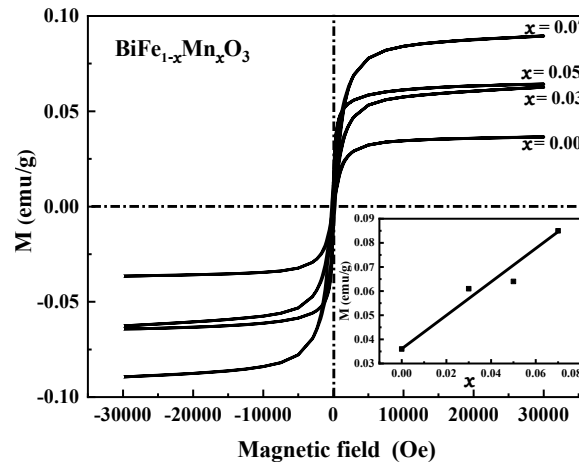

Fig. 5 Room temperature ($M − H$) hysteresis loop of $BiFe_{1-x}Mn_xO_3$ ($x = 0.00$, 0.03, 0.05 and 0.07) films, in which the insert shows the variation in Ms with Mn-doping concentration.

saturated magnetization (M_s) as a function of the Mn content (x). The M_s of the BFO ($x = 0.00$, 0.03, 0.05 and 0.07) films were approximately 0.036, 0.061, 0.064 and 0.085 emu/g, respectively, per total sample mass. The enhancement of magnetic properties attributed to the increase of Mn content, inducing more structural distortions, thus suppressing cycloid spin structure in the BFMO films [24], which coincides with the XRD results. According to Fig. 1(b), the increase in the Mn content shifted all of the peak positions towards the larger angle direction, thus revealing a more structural distortion.

Fig. 6 shows the absorption spectra in the wavelength range from 300–700 nm of BFMO films. All of the samples exhibited strong light absorption in
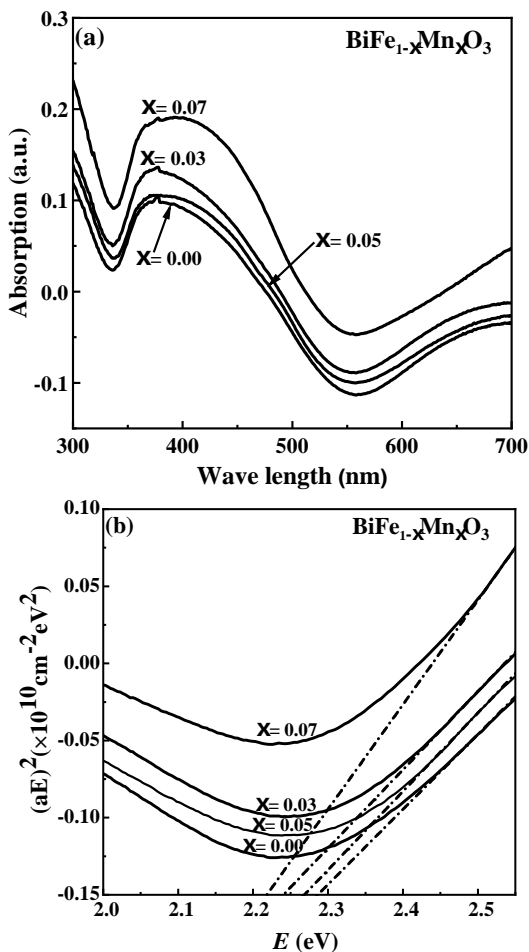
Fig. 6 (a) Absorption spectra and (b) band gaps of the BiFe$_{1-x}$Mn$_x$O$_3$ ($x = 0.00$, 0.03, 0.05 and 0.07) films.

both the UV and visible light regions (Fig. 6(a)), demonstrating that the as-prepared BFO could respond to visible light for the photocatalytic reaction. Compared to the BFO, the BFMO samples showed improved absorption in the visible light region, especially for the $x = 0.07$ sample. The optical absorbance properties were relevant to the electronic structure features and band gaps [29]. The optical band gaps (E_g) of the BFMO samples were determined by Tauc's law [30]. The BFMO films exhibited E_g values of 2.28 eV, 2.24 eV, 2.27 eV and 2.20 eV at Mn contents of $x = 0.00$, 0.03, 0.05 and 0.07, respectively (Fig. 6(b)). The E_g values clearly decreased with the Mn dopant possibly due to the energy levels of the doping ions entering the band gap and transitioning to impurity levels as the doping amount further increased, and resulting in narrow band gaps. Thus, the substitution of Mn

ions in the BFO film Fe sites resulted in decreased E_g values [31]. Smaller BFMO film E_g values resulted in wider visible light regions for the photovoltaic devices.

In summary, BiFe$_{1-x}$Mn$_x$O$_3$ ($x = 0.00$, 0.03, 0.05 and 0.07) films were synthesized by the sol-gel method. The XRD analysis revealed effectiveness of Mn doping in enhancing the film crystallinity. In particular, as the amount of doping increased, the grain size first decreased and then increased. The AFM images showed that the roughness of the BFMO film depended on the doping content. Meanwhile, the saturated magnetization of the BFMO films increased with the Mn content, which indicates the promising effectiveness of the BFMO film as a candidate for multiferroic device applications. The film band gap decreased from 2.28 eV to 2.20 eV, suggesting that the smaller band gap of the BFMO film resulted in a wider visible light region for photovoltaic devices.

REFERENCES

1. Tyagi M, Chatterjee R, Sharma P (2015) Structural, optical and ferroelectric behavior of pure BiFeO$_3$ thin films synthesized by the sol-gel method. *J Mater Sci-Mater El* **26**, 1987–1992.
2. Hong NH, Huong NT, Kim TY, Goumri-Said S, Kanoun MB (2015) Tuning magnetic properties of BiFeO$_3$ thin films by controlling rare-earth doping: experimental and first-principles studies. *J Phys Chem C* **119**, 14351–14357.
3. Xu X, Tan GQ, Ren HJ, Ao X (2013) Structural, electric and multiferroic properties of Sm-doped BiFeO$_3$ thin films prepared by the sol-gel process. *Ceram Int* **39**, 6223–6228.
4. Khalid A, Ali M, Mustafa GM, Atiq S, Ramay SM, Mahmood A, Naseem S (2016) Structural and dielectric properties of sol-gel synthesized (Mn, Cu) co-doped BiFeO$_3$ ceramics. *J Sol-Gel Sci Techn* **80**, 814–820.
5. Sun Y, Sun ZB, Wei R, Huang YX, Wang LL, Leng J, Xiang P, Lan M (2018) First principles study of the magnetic properties and charge transfer of Ni-doped BiFeO$_3$. *J Magn Magn Mater* **449**, 10–16.
6. Tan QH, Wang QJ, Liu YK (2018) Magnetic properties and spontaneous polarization of La-, Mn- and N-doped tetragonal BiFeO$_3$: A first-principles study. *Materials* **11**, ID 985.

7. Arora M, Kumar M (2015) Structural, magnetic and optical properties of Ce substituted BiFeO$_3$ nanoparticles. *Ceram Int* **41**, 5705–5712.

8. Basu S, Hossain SKM, Chakravorty D, Pal M (2011) Enhanced magnetic properties in hydrothermally synthesized Mn-doped BiFeO$_3$ nanoparticles. *Curr Appl Phys* **11**, 976–980.

9. Yan HR, Deng HM, Ding NF, He J, Peng L, Sun L, Yang PX, Chu JC (2013) Influence of transition elements doping on structural, optical and magnetic properties of BiFeO$_3$ films fabricated by magnetron sputtering. *Mater Lett* **111**, 123–125.

10. Si HY, Lu WL, Chen JS, Chow GM, Sun XG, Zhao JJ (2013) Hydrothermal epitaxial multiferroic BiFeO$_3$ thick film by addition of the PVA. *J alloy Compd* **577**, 44–48.

11. Soram BS, Ngangom BS, Sharma HB (2012) Effect of annealing temperatures on the structural and optical properties of sol-gel processed nanocrystalline BiFeO$_3$ thin films. *Thin Solid Films* **524**, 57–61.

12. Zhou YH, Fan YF, Wang ZC, Mao WW, Weng YK, Zhang J, Pu Y, Yang JP, et al (2019) Effect of non-metallic X (X=F, N, S) and Cr co-doping on properties of BiFeO$_3$: A first-principles study. *Phys Lett A* **383**, 383–388.

13. Sun W, Wang WX, Chen D, Zhang GB, Cheng ZX, Wang YX (2019) First-principles investigation on tunable electronic properties and magnetism by polarization in PbTiO$_3$/BiFeO$_3$ 2D ferroelectric heterostructures. *J Mater Chem C* **7**, 463–473.

14. Guo RQ, Fang L, Dong W, Zheng FG, Shen MR (2010) Enhanced photocatalytic activity and ferromagnetism in Gd doped BiFeO$_3$ nanoparticles. *J Phys Chem C* **114**, 21390–21396.

15. Wang DW, Wang ML, Liu FB, Cui Y, Zhao QL, Sun HJ, Jin HB, Cao MS (2015) Sol-gel synthesis of Nd-doped BiFeO$_3$ multiferroic and its characterization. *Ceram Int* **41**, 8768–8772.

16. Yang SJ, Zhang FQ, Xie XB, Sun HJ, Zhang LP, Fan SH (2018) Enhanced leakage and ferroelectric properties of Zn-doped BiFeO$_3$ thin films grown by sol-gel method. *J Alloy Compd* **734**, 243–249.

17. Gupta S, Tomar M, Gupta V (2013) Raman spectroscopy of nanocrystalline Mn-doped BiFeO$_3$ thin films. *J Exp Nanosci* **8**, 261–266.

18. Brahmi M, Amami M, Hassen RB (2016) Enhancement in magnetic properties of Mg-doped strontium-substituted bismuth ferrite prepared by solid-state and sol-gel methods. *J Supercond Nov Magn* **29**, 2359–2365.

19. Dong GH, Tan GQ, Liu WL, Xia A, Ren HJ (2014) Effect of Tb doping on structural and electrical properties of BiFeO$_3$ thin films prepared by sol-gel technique. *J Mater Sci Technol* **30**, 365–370.

20. Tuersun Y, Rouzhahong Y, Maimaiti M, Salamu A, Xiaerding F, Mamat M, Qun J (2018) First-principles studies on mechanical, electronic, magnetic and optical properties of new multiferroic members BiLaFe$_2$O$_6$ and Bi$_2$FeMnO$_6$: originated from BiFeO$_3$. *Curr Appl Phys* **18**, 1473–1479.

21. Wang LC, Wang ZH, He SL, Li X, Lin PT, Sun JR, Shen BG (2012) Enhanced magnetization and suppressed current leakage in BiFeO$_3$ ceramics prepared by spark plasma sintering of sol-gel derived nanoparticles. *Condens Matter* **407**, 1196–1202.

22. Wang TT, Deng HM, Cao HY, Zhou WL, Weng GE, Chen SQ, Yang PX, Chu JH (2017) Structural, optical and magnetic modulation in Mn and Mg co-doped BiFeO$_3$ films grown on Si substrates. *Mater Lett* **199**, 116–119.

23. Raj CA, Muneeswaran M, Jegatheesan P, Giridharan NV, Sivakumar V, Senguttuvan G (2013) Effect of annealing time in the low-temperature growth of BFO thin films spin coated on glass substrates. *J Mater Sci-Mater El* **24**, 4148–4154.

24. Liu YQ, Qi J, Zhang YL, Wang YH, Feng M, Zhang JK, Wei MB, Yang JH (2018) Surface agglomeration is beneficial for release of magnetic property via research of rare earth (RE) element-substitution. *Appl Surf Sci* **427**, 745–752.

25. Dong GH, Tan GQ, Luo YY, Liu WL, Ren HJ, Xia A (2014) Optimization of the multiferroic BiFeO$_3$ thin films by divalent ion (Mn, Ni) co-doping at B-sites. *Mater Lett* **118**, 31–33.

26. Hu ZJ, Chen D, Wang S, Zhang N, Qin LS, Huang YX (2017) Facile synthesis of Sm-doped BiFeO$_3$ nanoparticles for enhanced visible light photocatalytic performance. *Mat Sci Eng B* **220**, 1–12.

27. Han YL, Liu WF, Xu XL, Guo MC, Zhang XN, Wu P, Rao GH, Wang SY (2017) Room-temperature multiferroic and optical properties in Ba and Rb codoped BiFeO$_3$ nanoparticles. *J Alloy Compd* **695**, 2374–2380.

28. Hu ZQ, Li MY, Liu J, Pei L, Wing J, Yu BF, Zhao XZ (2010) Structural transition and multiferroic properties of Eu-doped BiFeO$_3$ thin films. *J Am Ceram Soc* **93**, 2743–2747.

29. Liu J, Deng HM, Zhai XZ, Lin T, Meng XJ, Zhang YY, Zhou WL, Yang PX, et al (2014) Influence of Zn doping on structural, optical and magnetic properties of BiFeO$_3$ films fabricated by the sol-gel technique. *Mater Lett* **133**, 49–52.

30. Wang ZC, Ma YH, Zhou YH, Hu RY, Mao WW, Zhang J, Min YG, Yang JP, et al (2017) Multiferroic-and bandgap-tuning in BiFeO$_3$ nanoparticles via Zn and Y co-doping. *J Mater Sci- Mater El* **28**, 11338–11345.

31. Kuang DH, Tang P, Wu XH, Yang SH, Ding XD, Zhang YL (2016) Structural, optical and magnetic studies of (Y, Co) co-substituted BiFeO$_3$ thin films. *J Alloy Compd* **671**, 192–199.